Available online at www.sciencedirect.com

ScienceDirect

Procedia IUTAM 21 (2017) 86 – 93

Procedia IUTAM

www.elsevier.com/locate/procedia

2016 IUTAM Symposium on Nanoscale Physical Mechanics

Size-dependent Phase Transformation and Fracture of ZnO Nanowires

Jianying He[a,] *, Jianyang Wu[b], Shijo Nagao[c], Lijie Qiao[d], Zhiliang Zhang[a]

[a]*NTNU Nanomechanical Lab, Department of Structural Engineering, Norwegian University of Science and Technology (NTNU), 7491, Trondheim, Norway*

[b]*Department of Physics, Research Institute for Biomimetics and Soft Matter, Xiamen University, 361005, Xiamen, China*

[c]*Institute of Scientific and Industrial Research, Osaka University, 8–1 Mihogaoka, Ibaraki, Osaka, Japan*

[d]*Corrosion and Protection Center, Key Laboratory of Environmental Fracture (Ministry of Education), University of Science and Technology Beijing, 100083, Beijing, China*

Abstract

The structural and mechanical properties of ZnO nanowires (NWs) have been systematically investigated by using molecular dynamic simulations based on the empirical Buckingham potential. Under tensile loading in <0001> direction, ZnO NWs undergo four-stage deformation: elastic stretching of initial Wurtzite structure, Wurtzite to body-centered tetragonal (BCT) phase transformation, stretching of the resulting BCT structure and eventually brittle fracture. The entire deformation process is significantly size dependent. As the NW size decreases, the Young's modulus dramatically increases. The critical stress for both phase transformation and fracture decreases while the critical strain increases with increasing the NW size; both converge to constant values when the size is sufficiently large. The strain energy density for the initiation of phase transformation appears independent of the size, which implies that the size-dependent phase transformation is dominated by the size effect of the Young's modulus.

Peer-review under responsibility of organizing committee of Institute of the 2016 IUTAM Symposium on Nanoscale Physical Mechanics

Keywords: Zinc oxide; size effect; phase transformation; molecular dynamics

* Corresponding author. Tel.: +47-735-94686; fax: +47-735-94701.
E-mail address: jianying.he@ntnu.no

Peer-review under responsibility of organizing committee of Institute of the 2016 IUTAM Symposium on Nanoscale Physical Mechanics
doi:10.1016/j.piutam.2017.03.041

1. Introduction

Quasi-one-dimensional nanostructures made of semiconducting materials possess large potential applications in electronic and electromechanical devices due to their unique mechanical and electrical properties associated with their finite size[1]. In particular, Zinc oxide (ZnO) nanostructures have received more attention due to their excellent performance in electronic, ferroelectric, piezoelectric and optical applications[2]. In recent years, a great variety of ZnO nanostructures, such as nanowires (NWs), nanorods, nanobelts and nanorings, have been synthesized and employed as ultra-sensitive sensors, nano-resonators, field effect transistors and nano-cantilevers in diverse technologies of environmental monitoring, bio-medical systems and communications[3-7]. The structural, mechanical, optical and electric as well as piezoelectric properties of ZnO have been investigated experimentally. As regards mechanical properties, the reported values of Young's modulus vary in a large range from 20 GPa to 220 GPa by means of bending deflection, bending resonance, nanoindentation and tensile stretching[8-11]. The lack of agreement on experimental results is attributed to crystalline structure, geometry condition, sample manipulation, instrument calibration, and so on. While experimental evaluations at the nano-scale are full of challenges and uncertainties, molecular simulations provide an alternative way to study mechanical properties of ZnO nanostructures[11-15]. An interesting size effect on elastic properties of ZnO has been found in both experiments and numerical simulations[11]. The involved mechanism for the size effect has been qualitatively discussed and attributed to surface stress and surface elasticity due to the surface contraction correlated with the bond length of surface atoms[12-16]. Based on these surface analyses, a core–shell model has been proposed to explain the size effect, introducing a surface shell with constant thickness that contributes more significantly to the entire mechanical property for smaller nanostructures than that for larger ones[9]. A novel transformation from original Wurtzite to body-centered tetragonal (BCT) phase has been numerically discovered on ZnO nanowires under tension along with <0001> axial orientation whereas some studies claim that there is no such phase transformation[12,14]. To clarify those controversial results in experiments and simulations, we have performed here large-scale molecular dynamics (MD) simulations to investigate the mechanical properties of ZnO NWs using LAMMPS (Large-Scale Atomic/Molecular Massively Parallel Simulator) code. In addition to the elastic property, the size effect on the Wurtzite–BCT phase transformation as well as the fracture behavior of ZnO NWs under uniaxial tension has been scrutinized.

2. Computational methods

Wurtzite ZnO NWs oriented in <0001> with hexagonal cross-section were generated (see Fig.1) where the lattice constant a = 3.2501 Å, c = 5.2071 Å, and internal parameter u = 0.3817[17]. The lateral dimension of the NWs varied from 1.0, 1.8, 2.4, 3.0, and 5.0 to 10 nm, while the length was kept constant 10.4 nm. Empirical Buckingham potential with Binks parameters was adopted to describe the short-range atomic interactions in which the cut-off was set to 10 Å[18]. This potential has successfully reproduced the crystal parameters, elastic constants and dielectric constants of bulk ZnO[11-13]. As for the long-range Coulombic force, Ewald summation method was used for NWs with D < 10 nm; otherwise Particle-Particle Particle-Mesh method (PPPM) developed by Hockney and Eastwood was employed[19,20]. The latter one had a major advantage in saving computing time and was confirmed to give identical results on the NWs with D = 1.8, 2.4 and 3.0 nm, except slightly more fluctuations at the beginning of deformation. Periodic boundary conditions were imposed on the three directions for the accurate Coulombic force calculation, while a sufficiently large gap along lateral directions was given to avoid interactions between neighboring NWs. Prior to tensile loading, an annealing process with an integration time step of 1 fs was performed to relax the NWs under the ambient pressure (*NPT*) in <0001> direction using the Nose-Hoover thermostat and barostat[21,22]. The temperature of the NWs was once raised from 5 K to 300 K within 10 ps, and equilibrated at 300 K for 5 ps. The annealed system was then quenched down to 5 K in 5 ps, and equilibrated at 5 K for 10 ps. This annealing and quenching process was sufficient to stabilize the ZnO NWs with the given lattice constants and the employed atomic potential. The uniaxial tensile strain was applied to the NWs by extending the length of periodicity along the tension direction, under *NVT* conditions at 5 K to reduce the thermal vibration. The strain rate of 0.001/ps was retained to deform the NWs up to 30 % strain. The tensile stresses were calculated by the Virial theorem and the stress−strain relationships were obtained[23].

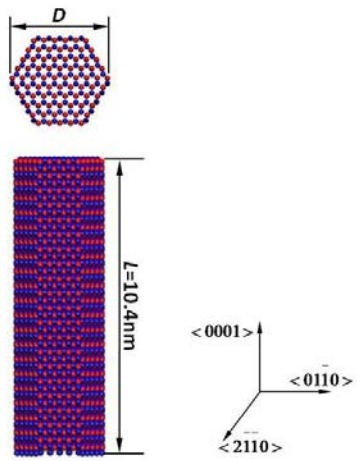

Fig. 1. The geometry of ZnO nanowires prior to annealing. Blue spheres represent zinc atoms and red ones oxygen atoms (same applies to the following Fig.s).

3. Results and discussion

The typical stress–strain curve obtained for the intermediate size D = 3.0 nm NW is plotted in Fig. 2 (a), and the corresponding morphological configuration projected on $(2\bar{1}\bar{1}0)$ plane during deformation are shown in Fig. 2 (b) – (e). The results suggest that the deformation process of ZnO NWs consists of the four stages: elastic stretching represented by the initial linear region (stage I), a phase transformation indicated by the stress relaxation (stage II), stretching of the structure with a new phase (stage III), and eventual fracture by the secondary stress relaxation (stage IV). In the case of morphology observation, when the strain is 6 %, the deformation is presented simply by the stretching of the initial crystal lattice, as shown in Fig. 2 (c). As the strain increases to 12 %, where the first stress drop takes place, a drastic change of the crystalline structure is observed (see Fig. 2 (d)), confirming the phase transformation from Wurtzite to BCT structure[14]. This finding appears against the previous studies which claim that square cross-sectional ZnO NWs with <0001> growth direction do not show phase transformations and are relatively brittle with failure strains less than about 7 %[12,24]. After the phase transformation, no intermediate phase occurs during further deformation, and the NWs keep the BCT structure until its failure shown in Fig. 2 (e).

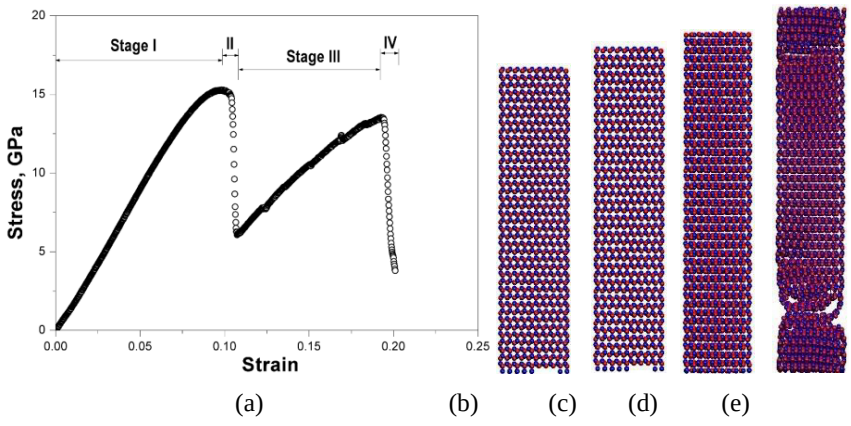

Fig. 2. The deformation process of the 3.0 nm ZnO nanowire: (a) the stress-strain curve; and (b) - (e) structure images projected on $(2\bar{1}\bar{1}0)$ at each strain of 0.0, 6.0, 12.0 and 20.0 %, respectively.

In order to better understand the phase transformation process of ZnO NWs, the atomic rearrangement on the projected section of $(2\bar{1}\bar{1}0)$ plane of 3.0 nm NW during the first stress relaxation is shown in Fig. 3 (a) – (d), and the detailed atom movement is explained in Fig. 3 (e) and (f). At 10.4 % strain, which is prior to the stress drop, the crystal structure of the NW is simply kept stretched Wurtzite. When the strain increases to 10.5 and 10.6 %, phase transformation from the Wurtzite to BCT structure initiates at the hexagonal corners close to the surface layer of the NW, and progresses toward the center. Further deformed to 10.7 % strain, the phase transformation is almost completed, and then the NWs are deformed with stretching the resulting BCT structure.

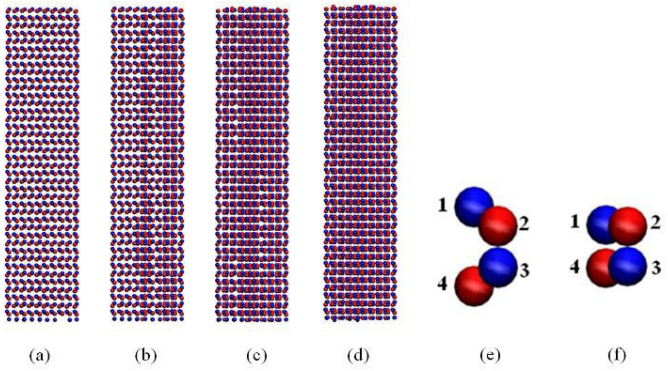

Fig. 3. The strain-induced Wurtzite to BCT phase transformation found in the 3.0 nm ZnO nanowire; (a) - (d) projected sections of $(2\bar{1}\bar{1}0)$ plane at the strain of 10.4, 10.5, 10.6 and 10.7 %; (e) and (f) atom movements as the strain increases from 10.4 to 10.7 %.

The stress–strain relationships for different sizes of ZnO NWs are compared in Fig. 4 (a). The mechanical response of ZnO NWs is significantly size dependent during the entire deformation process; not only the elastic behavior of the initial Wurtzite structure but also the mechanical response of the BCT structure after the phase transformation is influenced by the NW size. The stress relaxation due to phase transformation and fracture is also related to the NW size. For example, the smallest NW shows very sharp drops of stress, but the slope becomes milder with increasing NW size. This implies that larger NWs behave less brittle. In an effort to clarify the size effect, the Young's modulus and the critical stress/strain for the phase transformation and the fracture are summarized as a function of the NW size in Fig. 4 (b) – (d). The Young's modulus was obtained from the slope of the initial elastic region on the stress–strain curve. Critical stress and strain for phase transformation and fracture were directly read from the corresponding values at the starting points of the first and second stress relaxation, respectively.

Similar to MD studies in the literature, the size-dependent Young's modulus for <0001> oriented ZnO NWs states that the smaller the NW, the larger the Young's modulus[11]. The dashed line in Fig. 4 (b) represents the experimentally reported bulk value of 140 GPa for ZnO under tension in <0001> direction at 300 K[25]. The Young's modulus of NWs within the sampling size is always higher than that of the bulk counterpart. With increasing the NW size from 1.0 to 10.0 nm, the Young's modulus decreases from about 260 GPa to 145 GPa which approaches the bulk value. The confirmed size effect on the elastic modulus of ZnO NWs has been explained in connection with the fraction of the surface energy to the total energy[11]. The smaller NW has a larger portion of surface thus a higher ratio of the surface energy to the total, which results in more difficulties in deforming the smaller NW.

In Fig. 4 (c), it can be observed that the critical stress for phase transformation decreases with increasing size of NWs, while the critical strain increases. Within the range varied from 1.0 to 10.0 nm, the critical stress decreases about 40 % and the strain increases 43 %. This observation indicates that the larger NWs tend to retain Wurtzite phase so that a higher strain is required to initiate the phase transformation. This also indicates that the larger NWs behave less brittle, which is consistent with the above discussion. The trends of the critical stress and strain referred to different sizes of the NWs suggest that each converges to a constant value when the size is sufficiently large. To elucidate the size-dependent phase transformation, the strain energy density $u = U/V$ under the tensile load is introduced, where U is accumulated strain energy and V volume of the specimen. The critical strain energy density to initiate the Wurtzite–BCT phase transformation is expressed as:

$$u_{PT} = \int_0^{\varepsilon_{PT}} \sigma \cdot d\varepsilon \approx \frac{1}{2}\sigma_{PT}\varepsilon_{PT} \tag{1}$$

which can be evaluated either by the numerical integration of the obtained stress–strain curves, or by the linear approximation using the critical stress σ_{PT} and strain ε_{PT}. Fig. 5 presents u_{PT} with standard deviation determined for different sizes of NWs from the MD simulation. One can find that the variation of u_{PT} due to the NW size is less than 8 %, which is considerably smaller than that of critical stress and strain found in Fig. 4 (c). This strongly suggests that the critical strain energy required for the phase transformation is rather size independent, and can be a material constant of ZnO. Based on this assumption within the linear approximation of the Young's modulus *E*, the following equations can be deduced:

$$\varepsilon_{PT} = \sqrt{\frac{2u_{PT}}{E}}; \sigma_{PT} = \sqrt{2Eu_{PT}} \tag{2}$$

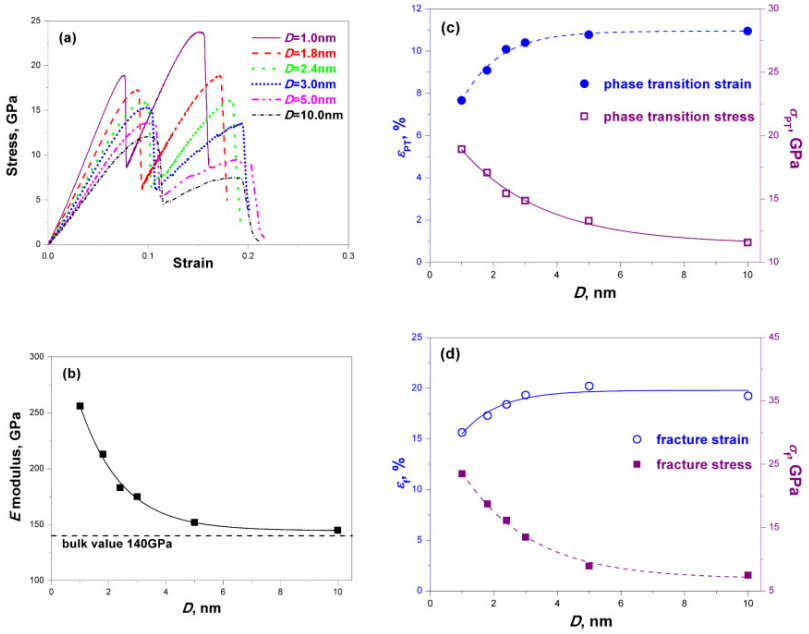

Fig. 4. Size dependence of mechanical properties of ZnO nanowires. (a) Stress-strain curves for sizes ranging from 1.0 to 10.0 nm; (b) Young's modulus; (c) the critical strain and stress for phase transformation; and (d) the fracture strain and stress.

Since Young's modulus *E* decreases with increasing NW sizes (see Fig. 4 (b)), the larger NWs experience a higher phase transformation strain and a relatively lower stress, as shown in Fig. 4 (c). The findings indicate that the size-dependent phase transformation of the ZnO NWs is dominated by the size effect of the Young's modulus.

Similar trend is found on the fracture stress and strain as that for phase transformation, where the size effect is more pronounced, as shown in Fig. 4 (d). When the NW size changes from 1.0 to 10.0 nm, the fracture stress reduces about 68 %. This is connected to the size effect on phase transformation. Because the deformation of the BCT structure starts right after the phase transformation, the analysis of the strain energy density for fracture is not applicable.

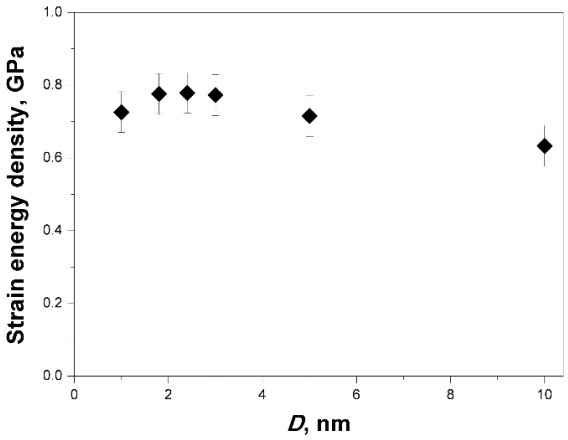

Fig. 5. The strain energy density of the ZnO NWs.

During the tension tests, the system temperature is kept constant 5 K at which atomic vibrations are well suppressed so that the thermal effect on the ductility is minimized. The ZnO NWs display brittle fracture at a relatively high strain over 15 %. The fracture morphologies of all tested NWs present with perfect cleavage along (0001) planes, as shown in Fig. 6. This cleavage fracture is unique for our hexagonal cross-sectional NWs, distinguished from the cylindrical NWs that exhibit super ductility[12], and also from the square cross-sectional NWs that display lower fracture strain around 6 %[15]. The main reason is that these two shapes of cross-sectional NWs were initially distorted into a twisted configuration and even an amorphous structure when the system energy was minimized during the equilibration. The crystal structures of ZnO NWs in these studies are highly defective prior to deformation, and hence these models could not be considered as Wurtzite structure. As confirmed by Fig. 2 (b), our NW models with hexagonal cross-section kept perfect Wurtzite crystalline structure after annealing. Moreover, the hexagonal ZnO NWs had smooth surfaces and homogenous cross-section over the entire wire structure, while the cylindrical ones often showed irregular shape in experiments[26,27].

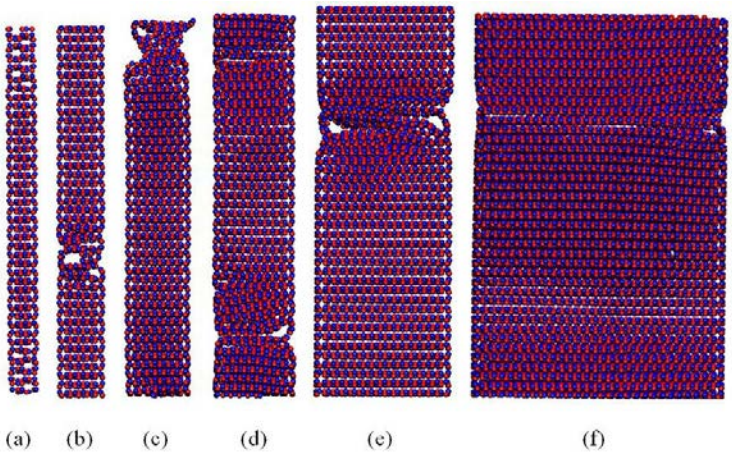

Fig. 6. (a) - (f) The fracture morphology of ZnO NWs with the size of 1.0, 1.8, 2.4, 3.0, 5.0 and 10.0 nm at the strain of 15.85, 17.55, 18.70, 19.75, 20.75 and 19.75 %, respectively.

The experimental study on ZnO nanostructures, however, has not yet confirmed the phase transformation predicted by the MD simulations. Several factors can be responsible for the discrepancy. One is that the strain rate in MD simulations is extremely high because of limited computer resource. In this study the tensile strain rate is 109 /s which is inconceivable in practical experiments. The key question is that if the phase transformation is induced by the high strain rate. The second explanation is that the loading cell in experiment is unable to catch the sudden stress relaxation associated to the phase transformation due to the limitation of mechanical devices. By means of in-situ mechanical testing in transmission electron microscopy (TEM) incorporating the electron diffraction pattern, it might help to determine the crystalline structure at different deformation levels. Another possible reason is that the NWs in experiments include many crystal defects, so that the imperfect structure cannot sustain large deformation, and the failure happens prior to the phase transformation. Finally, the different scale between the MD simulations and the experimental studies may cause this discrepancy. The MD simulations deal with the size in sub-nano and nano-scales while physical experiments limit the specimen size to tens of nanometers. Our study confirms the size of ZnO NWs is the key factor for the driving force to initiate the phase transformation, as discussed above.

4. Conclusions

In conclusion, size-dependent mechanical properties of ZnO NWs have been investigated computationally. The hexagon cross-sectional NWs can keep perfect crystalline structure during the initial equilibration and retain the initial Wurtzite structure prior to deformation. Under uniaxial tension, ZnO NWs experience a four-stage deformation process consisting of the elastic stretching of Wurtzite structure, the phase transformation from Wurtzite to BCT, the stretching of the BCT structure, and the cleavage fracture along (0001) plane. In addition to the size-dependent Young's modulus reported by previous studies, it is found that phase transformation and fracture properties are significantly influenced by the size of NWs. The critical stresses for both phase transformation and fracture drastically increase while the critical strain decreases as the NW size decreases. It suggests that larger NWs attempt to keep the original Wurtzite structure comparing with smaller ones. The strain energy density for the initiation of phase transformation is independent of the NW size and can be considered as a material constant.

Acknowledgements

The authors would like to thank NOTUR – The Norwegian Metacenter for Computational Science for the support of computational resources with project number NN9110k and NN9391k.

References

1. Lu JG, Chang P, Fan Z, Quasi-one-dimensional metal oxide materials-Synthesis, properties and applications. *Mater Sci Eng R*, 2006;**52**:49–91.
2. Wang ZL, ZnO nanowires and nanobelts platform for nanotechnology. *Mater Sci Eng R*, 2009;**64**:33–71.
3. Kong XY, Ding Y, Yang R, Wang ZL, Single-crystal nanorings formed by epitaxial self-coiling of polar nanobelts. *Science*, 2004;**303**:1348–1351.
4. Gao PX, Ding Y, Mai W, Hughes WL, Lao CS, Wang ZL, Conversion of zinc oxide nanobelts into superlattice-structured nanohelices. *Science*, 2005;**309**:1700–1704.
5. Menzel A, Komin K, Yang Y, Guder F, Trouillet V, Werner P, Zacharias M, Ultra-long zinc oxide nanowires and boron doping based on ionic liquid assisted thermal chemical vapor deposition growth. *Nanoscale*, 2015;**7**:92-97.
6. Cheng JJ, Nicaise SM, Berggren KK, Gradecak S, Dimensional Tailoring of Hydrothermally Grown Zinc Oxide Nanowire Arrays. *Nano Lett*, 2016;**16**:753-759.
7. Cao Z, Cao X, Guo H, Li T, Jie Y, Wang N, Wang ZL, Piezotronic Effect Enhanced Label-Free Detection of DNA Using a Schottky-Contacted ZnO Nanowire Biosensor. *ACS Nano*, 2016;**10**:8038-8044.
8. Bai XD, Gao PX, Wang ZL, Wang EG, Dual-mode mechanical resonance of individual ZnO nanobelts. *Appl Phys Lett*, 2003;**82**:4806–4808.
9. Chen CQ, Shi Y, Zhang YS, Zhu J, Yan YJ, Size dependence of Young's modulus in ZnO nanowires. *Phys Rev Lett*, 2006;**96**:075505.
10. Hoffmann S, Ostlund F, Michler J, Fan HJ, Zacharias M, Christiansen SH, Ballif C, Fracture strength and Young's modulus of ZnO nanowires. *Nanotechnology*, 2007;**18**:205503.
11. Agrawal R, Peng B, Gdoutos EE, Espinosa HD, Elasticity size effects in ZnO nanowires — a combined experimental-computational approach. *Nano Lett*, 2008;**8**:3668–3674.

12. Kulkarni J, Zhou M, Ke FJ, Orientation and size dependence of the elastic properties of zinc oxide nanobelts. *Nanotechnology*, 2005;**16**:2749–2756.
13. Hu J, Liu XW, Pan BC, A study of the size-dependent elastic properties of ZnO nanowires and nanotubes. *Nanotechnology*, 2008;**19**:285710.
14. Agrawal R, Peng B, Espinosa HD, Experimental-computational investigation of ZnO nanowires strength and fracture. *Nano Lett*, 2009;**9**:4177–4183.
15. Dai L, Cheong WCC, Sow CH, Lim CT, Tan VBC, Molecular dynamics simulation of ZnO nanowires: size effect, defects and super ductility. *Langmuir*, 2010;**26**:1165–1171.
16. Miller RE, Shenoy VB, Size-dependent elastic properties of nanosized structural elements. *Nanotechnology*, 2000;**11**:139–147.
17. Kisi EH, Elcombe MM, u parameters for the Wurtzite structure of ZnS and ZnO using powder neutron diffraction. *Acta Crystallographica*, 1989;**45**:1867–1870.
18. Binks DJ, Computational modeling of zinc oxide and related oxide ceramics, PhD thesis, University of Surrey, Harwell, 1994.
19. Hockney R, Eastwood J, Computer simulation using particles, McGraw-Hill, New York. 1981.
20. Nikiforov I, Hourahine B, Aradi B, Frauenheim Th, Dumitrica T, Ewald summation on a helix: A route to self-consistent charge density-functional based tight-binding objective molecular dynamics. *J Chem Phy*, 2013;**139**:094110.
21. Nose S, A unified formulation of the constant temperature molecular dynamics methods. *J Chem Phys*, 1984;**81**:511–519.
22. Hoover WG, Canonical dynamics: equilibrium phase-space distributions. *Phys Rev A*, 1985;**31**:1695–1697.
23. Plimpton S, Fast parallel algorithms for short-range molecular dynamics. *J Comp Phys*, 1995;**117**:1–19.
24. Kulkarni J, Zhou M, Sarasamak K, Limpijumnong S, Novel phase transformation in ZnO nanowires under tensile loading. *Phys Rev Lett*, 2006;**97**:105502.
25. Simmons G, Wang H, Single crystal elastic constants and calculated aggregate properties, MIT Press: Cambridge, MA, 1971.
26. Wang Z L, Zinc oxide nanostructures: growth, properties and applications. *J Phys-Condens Mat*, 2004;**16**:R829–R858.
27. Wu ZY, Chen IJ, Lin YF, Chiu SP, Chen FR, Kai JJ, Lin JJ, Jian WB, Cross-sectional shpe modulation of physical properties in ZnO and Zn1-xCoxO nanowires. *New J Phys*, 2008;**10**:033017.